Electrochimica Acta 340 (2020) 135974

Contents lists available at ScienceDirect

Electrochimica Acta

journal homepage: www.elsevier.com/locate/electacta

# Stepwise enhancement on optoelectronic performances of polyselenophene via electropolymerization of mono-, bi-, and tri-selenophene

Baoyang Lu [a, 1], Nannan Jian [a, 1], Kai Qu [a], Faqi Hu [a], Ximei Liu [a, **], Jingkun Xu [a, *], Guoqun Zhao [a, b, ***]

[a] Flexible Electronics Innovation Institute, Jiangxi Science & Technology Normal University, Nanchang, 330013, China
[b] Key Laboratory for Liquid-Solid Structural Evolution and Processing of Materials (Ministry of Education), Shandong University, Jinan, 250061, Shandong, China

ARTICLE INFO

*Article history:*
Received 1 November 2019
Received in revised form
31 January 2020
Accepted 24 February 2020
Available online 27 February 2020

*Keywords:*
Conjugated polymers
Polyselenophene
Electrochemical polymerization
Flexible electronics
Electrochromics

ABSTRACT

Although much progress have been made on polyselenophenes-based molecular systems, the poor optoelectronic performance of parent polyselenophene still hamper both the fundamental understanding and practical applications of such materials due to the monomer instability during the polymerization process and the lack of suitable monomeric precursors. In this work, we develop an effective method to improve the optoelectronic performances and stability of parent polyselenophene by stepwise increasing the initial monomeric chain length for electrochemical polymerization. We find that the chain length increment of the monomeric structures from selenophene to bi- and tri-selenophenes dramatically reduces the electropolymerization potential and thus enables the formation of high quality polyselenophene films with better conjugated structures and less structural defects. As-formed polyselenophene from tri-selenophene reveals lowered optical band gap (1.72 eV), better redox activity and stability, and significantly improved electrochromic nature of reversible and stable color changes between red and blue with high performance including superior optical contrast up to 75%, high coloration efficiency up to 450 $cm^2$ $C^{-1}$, and very fast switching time (0.7 s for oxidation and 0.4 s for reduction). These advantageous properties of as-prepared polyselenophene films afford the successful fabrication of patterned flexible electrochromic devices, which exhibit reversible and stable color changes upon both doping-dedoping and mechanical bending.



## 1. Introduction

Conducting polymers, as a fast-growing field in material science, have attracted extensive scientific interests owing to their promising applications in diverse fields, such as organic field-effect transistors[1], organic solar cells [2], and polymer electrochromics [3,4], bioelectronics [5,6], soft actuators [7], etc. Numerous researches have been reported on a wide variety of conjugated molecular systems, such as polythiophenes, polypyrroles, and their derivatives, etc. Among them, polythiophene-based conjugated polymers have received special attention due to their unique optoelectronic properties and ease of functionalization[8–11]. As a close analogue of polythiophene, polyselenophene and its-based conjugated molecular systems, show several advantages including lower band gap, stronger intermolecular Se–Se interactions, more rigid conjugated backbone, higher polarizability and lower redox potentials[8,9]. These advantages make polyselenophenes-based molecular systems promising for various applications like field-effect transistors[1], solar cells [2], thermoelectric [12] and electrochromic devices [13].

Although tremendous advancement has been made on the science and technology for polyselenophenes in the last decade, parent polyselenophene still displays poor optoelectronic performances far from theoretical expectation due to the monomer

* Corresponding author.
** Corresponding author.
*** Corresponding author. Flexible Electronics Innovation Institute, Jiangxi Science & Technology Normal University, Nanchang, 330013, China.
*E-mail addresses:* lxm5812@163.com (X. Liu), xujingkun1971@yeah.net (J. Xu), zhaogq@sdu.edu.cn (G. Zhao).
[1] These authors contributed equally to this work.

https://doi.org/10.1016/j.electacta.2020.135974
0013-4686/

instability during the polymerization process and the lack of suitable monomeric precursors [8,9,14–16], which hinders both the fundamental understanding and practical applications of such materials. Apart from direct polymerization condition control in previous reports[8], the chemical structure modification of initial monomeric precursors is also expected to provide milder polymerization conditions if suitable monomeric precursors can be found. Unfortunately, little has been known on the effect of initial monomeric chain length on the polymerization behavior and the properties of the resultant polyselenophene. Owing to longer conjugated chain, oligoselenophenes like biselenophene and triselenophene have larger $\pi$ delocalization than selenophene and thus are much easier to oxidize while maintaining the conjugated selenophene moieties[8,14–16]. Therefore, we propose that increasing the initial monomeric precursor chain length is probably an effective approach to enhance the optoelectronic performances and stability of polyselenophene.

Herein, we carefully investigate the electropolymerization behavior of selenophene (Se), biselenophene (2Se), and triselenophene (3Se), and electropolymerize them to obtain the corresponding polyselenophene films. Multiple characterization techniques including spectral, morphological, electrochemical, as well as computational chemistry, have been used to systematically investigate the effect of monomeric precursor chain length on the electropolymerization behavior and the optoelectronic performances of the resultant polyselenophene films. Moreover, high quality polyselenophene film with excellent electrochromic performance has been achieved, allowing us to successfully fabricate patterned flexible electrochromic devices.

## 2. Experimental

### 2.1. Materials

Selenophene (99%; Shanghai Vita), dichloromethane ($CH_2Cl_2$, 99.8%; J&K), acetic acid ($CH_3COOH$, 99.8%; Shanghai Vita), *N*,*N*-dimethylformamide (DMF, 99.9%; Tianjin Bodi), *N*-bromosuccinimide (NBS, 98%; Tianjin Bodi), sodium bicarbonate ($NaHCO_3$, 99%; Sigma-Aldrich), chlorotributyltin ($SnBu_3Cl$, J&K), *n*-butyllithium (*n*-BuLi, 1.6 M in hexanes; J&K), lithium perchlorate ($LiClO_4$, 99%; J&K), acetonitrile ($CH_3CN$, 99.9%; Superdry, water $\leq$ 30 ppm, J&K), propylene carbonate (PC, 99.5%; Superdry, J&K), and poly(methyl methacrylate) (PMMA, J&K) were used directly without any purification. Tetrahydrofuran (THF, 99%; Shanghai Vita) was distilled from sodium benzophenone ketyl and used as the solvent for stannylization. Tetrakis(triphenylphosphine)palladium ($Pd(PPh_3)_4$, 99%; J&K) was used as the catalyst for Stille coupling. Tetrabutylammonium hexafluorophosphate ($Bu_4NPF_6$, 99%; Shanghai Vita) was employed as the supporting electrolyte for electrochemical polymerization and electrochromic tests after drying in vacuum for 24 h at 60 °C.

### 2.2. Characterization

By using a Bruker AV 400 NMR spectrometer, $^1H$ and $^{13}C$ NMR spectral measurements were taken with trimethylsilane (TMS) as the internal standard and $CDCl_3$ or DMSO-$d_6$ as the solvent. UV-vis absorption spectra of all samples were studied by a SPECORD 200 PLUS UV-vis spectrophotometer. An F-4500 fluorescence spectrophotometer was employed to determine the fluorescence spectra with the excitation and emission slit set at 5 nm. All quantum chemistry calculations were carried out by using the Gaussian 09 program package. Without symmetry constraints, the structures of the selenophene precursors were optimized with a hybrid Becke's-three-parameter Lee-Yang-Parr functional (B3LYP) in combination with the 6-31G(d,p) basis set (B3LYP/6-31G(d,p)). The energy gap ($E_{g,DFT}$) was calculated from the HOMO-LUMO gap. Electrochemical polymerization of all the precursors was performed by a Princeton Versa Stat 3 electrochemical workstation, with Pt wires (diameter: 1 mm) as the working/counter electrodes and an Ag/AgCl electrode as the reference electrode. The electrolytic solution was bubbled by nitrogen before every experiment to eliminate the effect of oxygen. In order to get sufficient polymer films for characterization, Pt sheet ($2 \times 1.5$ $cm^2$; as the working electrode) and ITO-coated glass sheet ($2 \times 2$ $cm^2$; as the counter electrode) were employed for the electrosynthesis. A Bruke Vertex 70 Fourier-transform infrared (FT-IR) spectrometer was used to record the infrared spectra of all the monomeric precursors and corresponding polyselenophene. Scanning electron microscope (SEM) images were taken by using a VEGA II-LSU scanning electron microscope. By combining an electrochemical workstation (Versa Stat 3) and a SPECORD 200 PLUS UV-vis spectrophotometer, spectroelectrochemistry and electrochromic kinetic studies of the polyselenophene films were systematically investigated in a custom-made electrochemical cell with an Ag/AgCl electrode as the reference electrode, indium tin oxide (ITO)-coated glass slide ($0.8 \times 2.5$ $cm^2$) as the working electrode, and a Pt wire (diameter: 1 mm) as the counter electrode, respectively.

### 2.3. Synthesis

2,2′-Biselenophene (2Se) and 2,2':5′,2″-terselenophene (3Se) were synthesized by Stille coupling (Fig. 1A). The detailed experimental procedures are illustrated as follows.

**2-Bromoselenophene.** Selenophene (0.50 g, 3.80 mmol), $CH_2Cl_2$ (4 mL), and $CH_3COOH$ (4 mL) were added into a flask and kept at 0 °C. Then *N*-bromosuccinimide (0.67 g, 3.80 mmol) was slowly added and the mixture was stirred for 2 h at 0 °C. After washing with deionized water and removing the solvent, 2-bromoselenophene (0.83 g, yield: 56%) was obtained as a colourless liquid by column chromatography. $^1H$ NMR (400 MHz, DMSO-$d_6$, $\delta$ ppm): 8.14 (d, 1H), 7.36 (s, 1H), 7.09 (s, 1H).

**2,5-Dibromoselenophene.** Selenophene (1.00 g, 7.63 mmol) and *N*-bromosuccinimide (3.00 g, 16.85 mmol) were added in tetrahydrofuran (50 mL). The solution was stirred for 12 h at room temperature. The solvent was removed and the crude product was purified by column chromatography to obtain 2,5-dibromoselenophene as a yellow liquid (2.16 g, yield: 95%). $^1H$ NMR (400 MHz, $CDCl_3$, $\delta$ ppm): 7.00 (s, 2H); $^{13}C$ NMR (400 MHz, $CDCl_3$, $\delta$ ppm): 132.99, 115.61.

**2,2′-Biselenophene (2Se).** 2-Bromoselenophene (0.80 g, 3.80 mmol), tributyl(2-selenophenyl)stannane (4.79 g, 11.40 mmol), tetrakis(triphenylphosphine)palladium(0) (44 mg, 10 mol%) and DMF (20 mL) were added in the flask and the mixture was refluxed for 8 h under argon atmosphere. Then the mixture was poured into distilled water (80 mL) and extracted with diethyl ether. The organic phase was washed with saturated $NaHCO_3$ solution and deionized water. 2,2′-Biselenophene (colorless plates, 0.71 g, yield: 71%) was purified by column chromatography. $^1H$ NMR (400 MHz, DMSO-$d_6$, $\delta$ ppm): 8.08 (d, 2H), 7.34 (s, 2H), 7.25 (s, 2H); $^{13}C$ NMR (400 MHz, DMSO-$d_6$, $\delta$ ppm): 144.17, 133.09, 130.41, 126.75.

**2,2':5′,2″-Terselenophene (3Se).** 2,5-Dibromoselenophene (0.30 g, 1.00 mmol), tributyl(2-selenophenyl)stannane (2.10 g, 5.00 mmol), tetrakis(triphenylphosphine)palladium(0) (116 mg, 10 mol%) and DMF (20 mL) were added in the flask and the mixture was refluxed for 8 h under argon atmosphere. Similarly, the mixture was poured into deionized water (80 mL) after the reaction, extracted with diethyl ether, and the organic phase was washed with saturated $NaHCO_3$ solution and deionized water. By

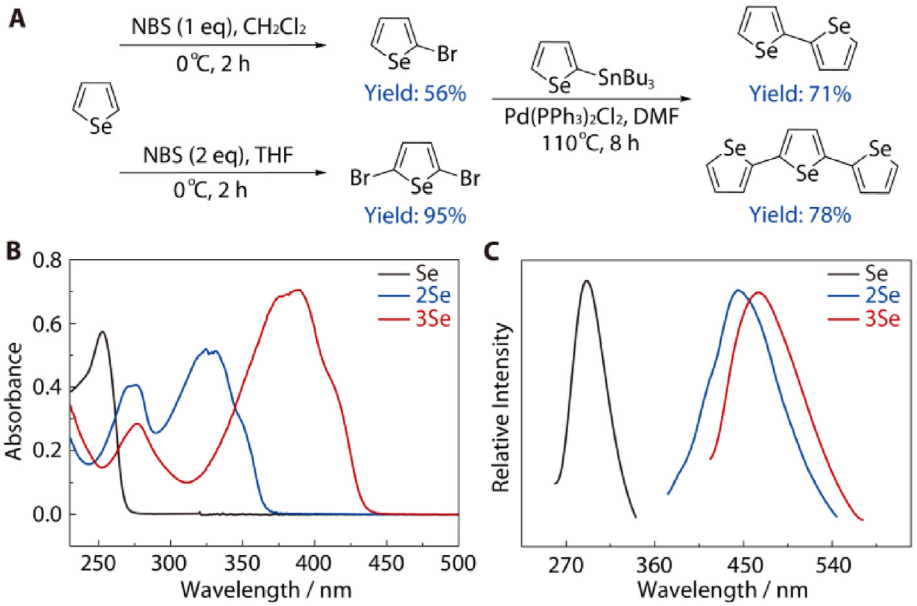


**Fig. 1. Synthetic route and photophysical properties.** (A) Synthetic procedure of 2,2′-biselenophene (2Se) and 2,2′:5′,2″-terselenophene (3Se). (B-C) UV-vis absorption spectra (B) and fluorescence emission spectra (C) of Se, 2Se, and 3Se dissolved in $CH_2Cl_2$.

purifying with column chromatography, 2,2′:5′,2″-terselenophene was obtained as a yellow leaflet (0.40 g, 78%). $^1$H NMR (400 MHz, DMSO-$d_6$, $\delta$ ppm): 8.12 (d, 2H), 7.37 (d, 2H), 7.28 (s, 2H), 7.27 (s, 2H); $^{13}$C NMR (400 MHz, DMSO-$d_6$, $\delta$ ppm): 143.52, 142.64, 131.58, 130.51, 127.62, 126.98.

### 2.4. Flexible electrochromic device fabrication

Flexible electrochromic devices (ECDs) were assembled into the following configurations: ITO-PET/patterned electrochromic polyselenophene layer/gel electrolyte/ITO-PET. For the patterning, polyselenophene electrochromic layer was electrosynthesized on ITO-PET (working electrode) by using a stencil to obtain the patterned ITO area and was then rinsed with $CH_2Cl_2$ to remove residual monomeric precursors, oligomers and electrolyte. A Pt sheet ($2 \times 2$ cm$^2$) was used as the counter electrode and an Ag/AgCl electrode was employed as the reference electrode for the electrosynthesis, respectively. For the ECD fabrication, the gel electrolyte with a composition of 3.5 wt%: 85.5 wt%: 5.5 wt%: 5.5 wt% (ACN: PC: $LiClO_4$: PMMA), which was prepared by mixing each component and stirring for 12 h at 65 °C, was coated on the patterned electrochromic layer. After evaporation of ACN in the gel electrolyte, another ITO−PET sheet was covered as the top layer and sealed with room temperature vulcanized (RTV) silicone rubber (Ausbond). The thickness of the gel electrolyte layer was controlled by a Scotch magic tape (3M). Copper strips (double conductive copper foil tape, thickness: 0.1 mm) were used for wiring as the electrodes of the ECDs.

## 3. Results and discussion

### 3.1. Molecular design and synthesis

Oligoselenophenes like 2Se and 3Se show elongated conjugated chain lengths and would possibly improve the stability and electrochromic properties of polyselenophene. To synthesize oligoselenophenes, selenophene (Se) was used as the starting molecule (Fig. 1A) and $Pd(PPh_3)_4$ was employed as the catalyst for Stille coupling. Through the stannylization of selenophene at 2-position, tributyl(selenophen-2-yl)stannane was obtained and directly used for the next step without further purification [9,17,18]. Stille coupling of tributyl(selenophen-2-yl)stannane with 2-bromoselenophene and 2,5-dibromoselenophene gave us the target compounds 2Se and 3Se in satisfactory yields (typically more than 70%), respectively. Notably, the molecular structures of all the intermediates and final products were confirmed by $^1$H NMR and $^{13}$C NMR spectra (Figs. S1−S7 in Supporting Information).

### 3.2. Optical properties

To evaluate the optical properties of the selenophene precursors, UV-vis absorption spectra and fluorescence emission spectra of Se, 2Se and 3Se were examined in $CH_2Cl_2$ (Fig. 1B and C), and the relevant optical parameters are summarized in Table 1. The absorption maxima for 2Se ($\lambda_{max}$ = 326 nm) and 3Se ($\lambda_{max}$ = 381 nm) are bathochromically shifted compared to the absorption maximum of Se ($\lambda_{max}$ = 252 nm) (Fig. 1B), suggesting higher extended π-conjugation in 2Se and 3Se due to a certain charge transfer character of π−π* transition of the selenophene−selenophene motif [19−22]. Stepwise red shifts are also observed in the emission spectra of Se, 2Se and 3Se (Fig. 1C), with the emission peaks at 291 nm, 444 nm and 465 nm (Table 1), respectively. This phenomenon could also be attributed to stepwise increase of the conjugated precursor chain length, which is in good agreement with the results of UV-vis absorption spectra.

### 3.3. Electrochemical polymerization

The electropolymerization behaviors of Se, 2Se, and 3Se have been examined via cyclic voltammetry in $CH_2Cl_2$-$Bu_4NPF_6$ (0.1 mol L$^{-1}$). From the anodic oxidation curves (Fig. 2A), the oxidation onset potentials ($E_{onset}$) of 2Se (1.16 V vs Ag/AgCl) and 3Se (0.93 V vs Ag/AgCl) were dramatically reduced than that of Se (1.57 V vs Ag/AgCl) (Table 1). Stepwise increase in chain length of selenophene leads to futher delocalization of π electrons along the molecules, making the oxidation of 2Se and 3Se into corresponding radical cations much easier. Notably, the significantly lowered $E_{onset}$ for the electrochemical polymerization of selenophenes are

**Table 1**
Optical, electrochemical parameters, and DFT theoretical calculations of Se, 2Se, and 3Se.

| Precursor | $\lambda_{max,1}$ (nm) | $\lambda_{max,2}$ (nm) | $\lambda_{em}$ (nm) | $E_{HOMO,\ DFT}$ (eV) | $E_{LUMO,\ DFT}$ (eV) | $E_{g,\ DFT}$ (eV) | Dihedral angles (°) | $E_{onset}$ (V) |
|---|---|---|---|---|---|---|---|---|
| Se | 252 | – | 291 | −6.32 | −0.35 | 5.96 | – | 1.57 |
| 2Se | 272 | 326 | 444 | −5.45 | −1.39 | 4.06 | 0.13390 | 1.16 |
| 3Se | 275 | 381 | 465 | −5.11 | −1.83 | 3.28 | 0.01957 | 0.93 |

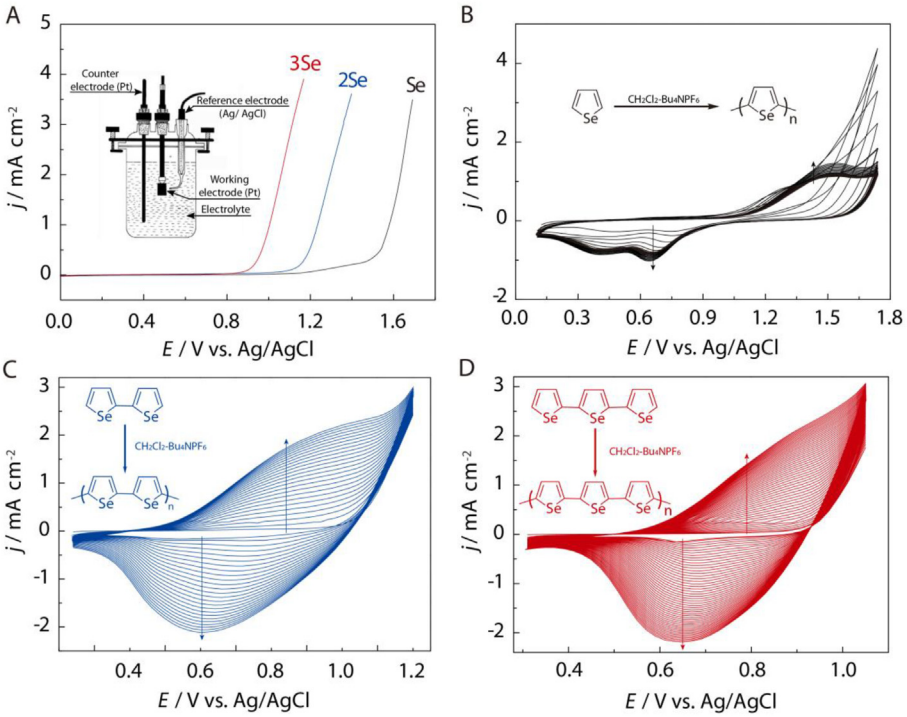


**Fig. 2. Electrochemical polymerization behavior.** (A) Anodic oxidation curves of 0.01 mol $L^{-1}$ Se, 2Se, and 3Se in $CH_2Cl_2$-$Bu_4NPF_6$ (0.10 mol $L^{-1}$). (B-D) Cyclic voltammograms of the electropolymerization of 0.01 mol $L^{-1}$ Se (B), 2Se (C), and 3Se (D) on Pt working electrodes in $CH_2Cl_2$-$Bu_4NPF_6$. Potential scan rate: 50 mV $s^{-1}$.

expected to effectively avoid the side reactions and overoxidation [23–26], which is quite beneficial to the formation of high quality polyselenophene films with much less structural defects.

Cyclic voltammetry (Fig. 2B–D) shows that the electropolymerization of 2Se and 3Se exhibits broad redox waves, which are similar with those of polythiophenes, polypyrrole and other classical conducting polymers previously reported[27]. Yet the CV curves of Se are not satisfactory with poorly defined redox waves and irregular increment (Fig. 2B), suggesting difficulty in the electropolymerization for Se. During the scanning process of 2Se and 3Se, dark polyselenophene films can be facilely obtained by visual inspection and current densities in the cyclic votammogram curves increase uniformly (Fig. 2C and D), indicating that the successful formation and gradual accumulation of polymers on the working electrode surface [28]. Meanwhile, the anodic and cathodic peak potentials shift to higher potentials owing to the increased electrical resistance required to balance the difference[29]. Overall, 2Se and 3Se are much easier to electropolymerize on the working electrode surface than Se due to the lowered onset oxidation potentials from the extended conjugation chain length.

For the polymer structure, morphology, and property characterization hereafter, potentiostatic electrolysis is employed to electrodeposit all the polyselenophene films. To optimize the applied potentials for electropolymerization, we recorded a set of current transients (chronoamperometric curves, see Fig. S8) during the electropolymerization of Se, 2Se, and 3Se at different applied potentials. After considering all the factors influencing the quality of the deposited polyselenophene film, such as negligible overoxidation, less structural defects, suitable polymerization rate, smooth and compact morphology, the selected applied potentials for Se, 2Se, and 3Se are 1.65 V, 1.35 V, and 1.1 V vs. Ag/AgCl in $CH_2Cl_2$-$Bu_4NPF_6$ (0.1 mol $L^{-1}$).

### 3.4. Structural characterization and surface morphology

#### 3.4.1. DFT theoretical calculations

In order to interpret the polymer structure and polymerization mechanism, the optimal molecular geometries and the frontier molecular orbital distributions (HOMO and LUMO) of Se, 2Se and 3Se were performed by quantum chemical calculations (Fig. 3A). Interestingly, both 2Se and 3Se show very planar structures with optimized dihedral angles close to 0°, indicating the highest possible π-electron coupling. This phenomenon will reduce the HOMO-LUMO gap of the corresponding polymers, and probably allow the achievement of polyselenophene with enhanced main chain planarity and higher performance. Notably, this finding also demonstrates that the selenophene moiety can be employed as an effective building block for the rational design of planar π-conjugated polymers. From the frontier molecular orbital theory, the electropolymerization mainly proceeds on the highest frontier molecular orbitals [30,31]. For all these selenophene precursors, the HOMO spreads dominantly over the α-positions of the selenophene

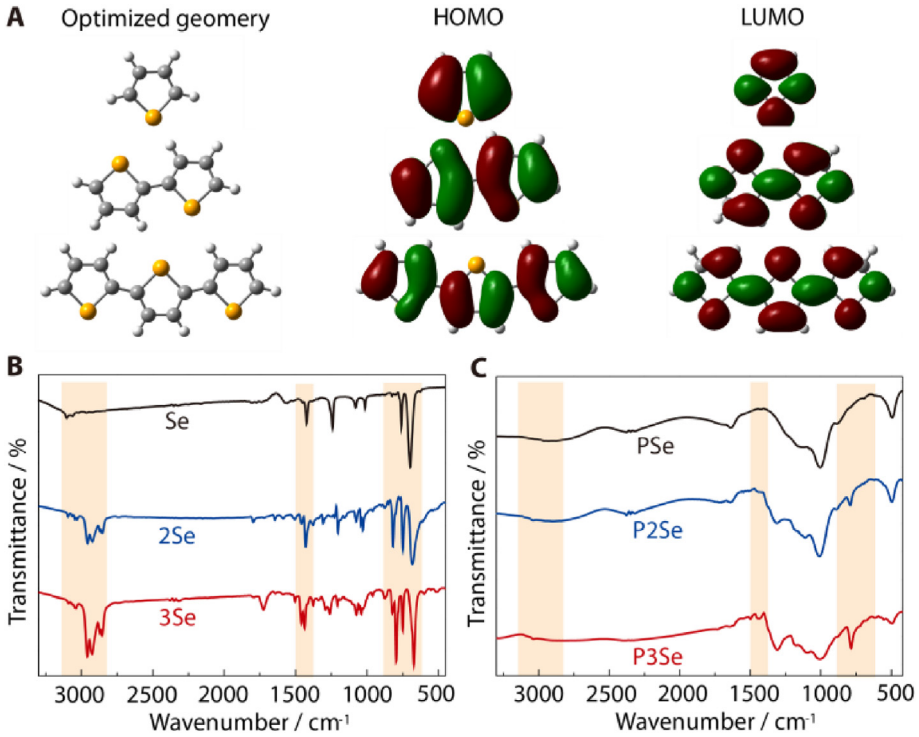


**Fig. 3. DFT theoretical calculations and structural characterization.** (A) Optimized molecular geometries and frontier molecular orbital distributions (HOMO and LUMO) for the selenophene precursors by DFT. (B-C) FT-IR spectra of the selenophene precursors (B) and their corresponding polyselenophenes (C).

ring, manifesting that the electropolymerization of Se, 2Se and 3Se occurs preferentially at α-positions. Furthermore, significant decrease in the band gap ($E_{g,\ DFT}$) can be observed along with the extension of initial conjugated chain lengths, namely, Se (5.96 eV), 2Se (4.06 eV), and 3Se (3.28 eV), in compliance with our previous calculations for conjugated oligomers [47].

### 3.4.2. FT-IR

In order to further clarify the electropolymerization mechanism and interpret the chemical structures of polyselenophene, we performed fourier transform infrared spectroscopy (FT-IR) of the selenophenone precursors and corresponding neutral polyselenophene, as shown in Fig. 3B. Compared to selenophene precursors, the vibrational absorption peaks of all the polymers are significantly broadened, probably due to the heterogeneous chain lengths and complicated configuration [32,33]. The main absorption peaks of PSe, P2Se and P3Se are almost consistent with varying peak shapes and intensities, indicating identical molecular structures of all these polyselenophene films. In the spectra of the selenophene precursors, the peaks at around 3200–3000 $cm^{-1}$ can be attributed to the = C–H stretching vibration in the selenophene ring, while these peaks are significantly weakened in the spectra of polyselenophene films. Moreover, in clear contrast with the precursors, all three polyselenophenes display a new absorption peak at 770–760 $cm^{-1}$, which is a characteristic out-of-plane bending vibration of adjacent = C–H bonding. These results confirm the electropolymerization of selenophene precursors at α-positions. Notably, the peak intensities of P2Se and P3Se in the range of 1600–1300 $cm^{-1}$ (stretching vibration of C=C and C–Se bonds) are obviously enhanced compared to those of PSe. This difference clearly evidences better conjugated structures of P2Se and P3Se with less structural defects than PSe, resulting from the elongated precursor chain length and much lower polymerization potentials as stated previously.

### 3.4.3. SEM

Scanning electron microscopy (SEM) of the electrodeposited polyselenophene has been employed for the morphological study (Fig. S8). At the magnification of ×5000, PSe film obtained by direct electropolymerization is thin and discontinuous, whereas P2Se and P3Se films are uniformly continuous and compact. Interestingly, typical coated polyselenophene nanowires could be found in P2Se film, which is rarely observed for electrodeposited conducting polymer films. P3Se film displays a compact surface with coral reefs, a common morphology occurrence for electrosynthesized conducting polymers[25,27,34,35]. Both P2Se and P3Se films reveal the large specific surface area, which is beneficial for the immigration/emigration of counterions during the doping-dedoping process. Furthermore, doped and dedoped polymer films display no obvious difference in morphology, demonstrating that the morphology of these polyselenophene films is not damaged upon doping-dedoping[19,22]. A few cracks in the SEM images for dedoped P2Se and P3Se films probably result from the fast evaporation of low boiling solvents like dichloromethane.

To further investigate its deposition mechanism of the polyselenophene nanowires, we studied the morphology evolution of P2Se films with varying deposition times (Fig. S9). For the nucleation at the initial stage of electropolymerization, P2Se deposits into a smooth morphology with random bulges on the ITO glass electrode (the deposition time of 2 s, Fig. S9A). With increasing polymerization time (10 s, Figs. S9B–E), the deposition rate on the bulges is faster than other parts, affording the gradual growth of polyselenophene into nanowires (Fig. S9E). Finally, the polymer deposits into a unique mixed morphology with nanowires and plates (Fig. S9F). We attribute this morphology to two-staged deposition: polyselenophene deposits mainly on the bulges to form nanowires after nucleation, and starts to deposit on the nanowires when the nanowires grow too long and fall against the surface. This unique deposition mode may be harnessed as a

template-free method to fabricate polyselenophene nanowires with fine control of polymerization time.

### 3.5. Electrochemistry of polyselenophene

Cyclic voltammetry of conducting polymer-modified electrodes is a simple yet effective method for detecting the electrochemical activity and stability of conducting polymer films[36–38]. The electrochemical properties of polyselenophene films are examined in blank $CH_2Cl_2$-$Bu_4NPF_6$ (0.10 mol $L^{-1}$), as illustrated in Fig. 4. Similar to those results for typical conducting polymers, these polyselenophene films exhibit broad anodic-cathodic waves (Fig. 4A–C) with basically same redox potential windows in the range of 0.2–1.4 V, which are similar with its analogue polythiophene[39–43]. Such broad redox waves of these polyselenophene films could be attributed to the following reasons: (1) the slow movement of counter ions in the polymer film; (2) the capacitance changes of the polymer film during the potential scanning; (3) wide chain length distribution of such polyselenophene; (4) inevitable structural defects such as α-β and β-β coupling among selenophene moieties during the polymerization process. Additionally, the redox peak current density shows a good linearity correlation with the potential scan rate (Fig. 4D–F), indicating that these polyselenophene films are well attached to the working electrode and the doping-dedoping processes are non-diffusionally controlled and reversible [19,20,22,25,26]. Compared to PSe, the redox current density values of both P2Se and P3Se are almost identical, and the linearity fitting of the redox current density versus potential scan rate for P2Se and P3Se are even better with the $R^2$ values closer to 1, indicating better electrochemical activity induced by increasing the precursor chain lengths.

From the cyclic voltammogram curves, we can also observe an obvious hysteresis in the redox peak potentials of polyselenophene, that is, the oxidation and reduction peak potentials drift at varying potential scan rates (Fig. 4A–C). Accompanying with the stepwise decrease in potential scan rates, the oxidation potentials of polyselenophene drop down gradually yet the reduction potentials rise step by step with the whole redox potential window of polyselenophene decreases correspondingly. This phenomenon is due to the competition between the scan rates and the migration rate of counter ions. Note that the peak potential drift of electrodeposited conducting polymers is difficult to interpret by using conventional kinetic diffusion theories (ion diffusion theory or interface charge transfer process). The main reasons of this phenomenon are generally as follows: different forms of electron transfer, local rearrangement of conducting polymer chains, interconversion among various conducting states, and mutual electron transfer between interfaces such as metal/polymer and polymer/solution interfaces.

Long-term electrochemical stability of these polyselenophene films is also recorded at the constant scan rate of 150 mV $s^{-1}$ in blank $CH_2Cl_2$-$Bu_4NPF_6$ electrolyte. As shown in Fig. 4G–I, both P2Se

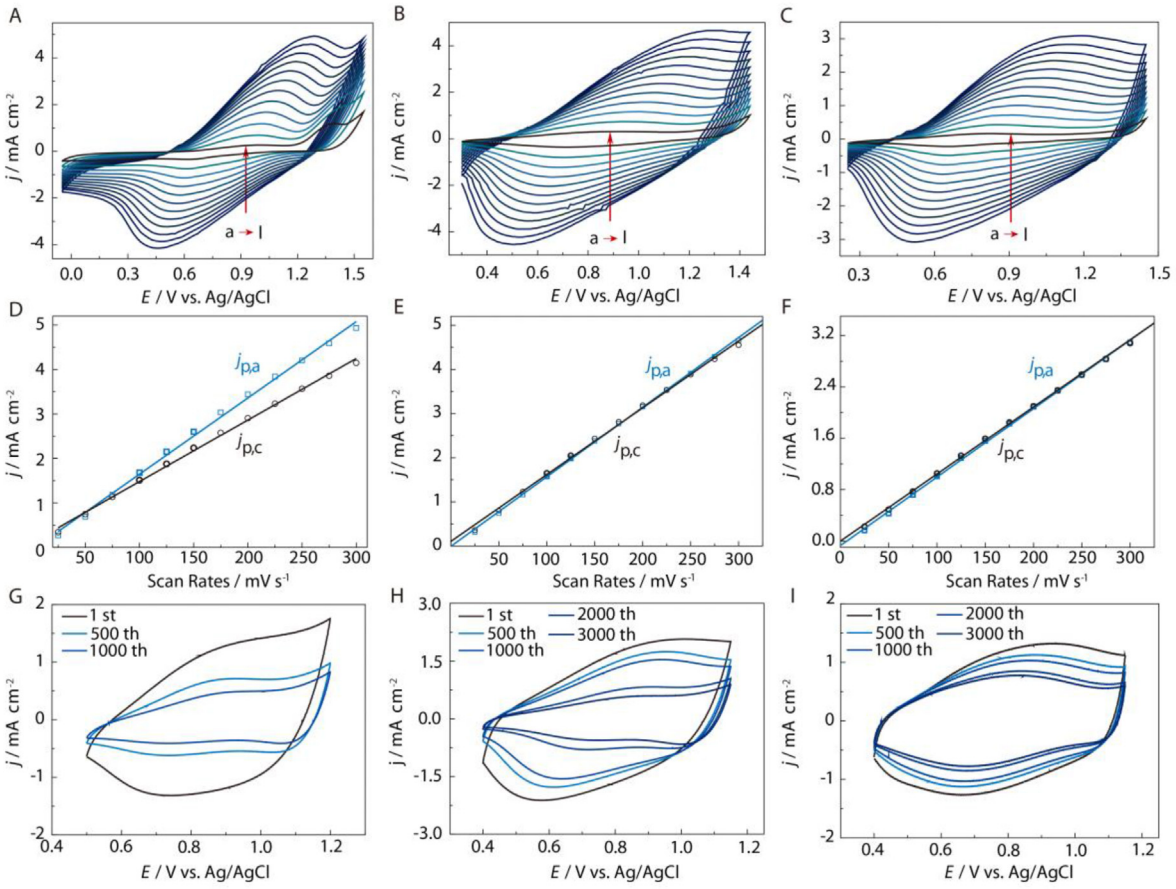


**Fig. 4. Electrochemistry of polyselenophenes.** (A-C) Cyclic voltammograms of PSe (A), P2Se (B), and P3Se (C) modified Pt electrodes in blank $CH_2Cl_2$-$Bu_4NPF_6$ (0.10 mol $L^{-1}$) at potential scan rates of 300 (a), 275 (b), 250 (c), 225 (d), 200 (e), 175 (f), 150 (g), 125 (h), 100 (i), 75 (j), 50 (k), and 25 (l) mV $s^{-1}$. (D-F) Plots of peak current densities *vs.* scan rates for PSe (D), P2Se (E), and P3Se (F). $j_p$ denotes peak current density, and $j_{p,a}$ and $j_{p,c}$ are the anodic and cathodic peak current density, respectively. (G-I) Long-term cyclic voltammograms of PSe (G), P2Se (H), and P3Se (I) in blank $CH_2Cl_2$-$Bu_4NPF_6$ (0.10 mol $L^{-1}$) at the constant potential scan rate of 250 mV $s^{-1}$.

and P3Se display superior redox stability than PSe, and P3Se reveals the best stability with retaining around 61% of its electroactivity after 3000 cycling. Such performance probably results from their better conjugated structures with less structural defects as mentioned previously.

### 3.6. Spectroelectrochemistry

The spectroelectrochemical method can realize the in-situ UV scanning of conducting polymer films at varying potentials and record the accompanying changes in chemical structure and physiochemical properties during the doping/dedoping process [19,20,22]. The electronic structure information can also monitor the changes in optical properties of conducting polymers upon doping/dedoping. Therefore, the spectroelectrochemistry of PSe, P2Se and P3Se films from the fully reduced state to the oxidized state is recorded in blank $CH_2Cl_2$-$Bu_4NPF_6$ (0.10 mol $L^{-1}$) (Fig. 5A–C).

Compared to the selenophene precursors (Fig. 1B and C), polyselenophene films coated on ITO glass display a dominant single-band absorption red-shifted to longer wavelengths (Fig. 5A–C) in the neutral state, owing to the increased conjugated polymer chain length. With increasing the precursor chain length from Se to 3Se, the maximum absorption peak of polyselenophene shifts bathochromically from 450 nm for PSe to 515 nm for P3Se, and the optical band gap ($E_g$) of the corresponding polyselenophene is gradually reduced from 1.92 eV (PSe) to 1.86 eV (P2Se) and 1.72 eV (P3Se), respectively. Notably, the band gap values of P2Se and P3Se are also lower than polyselenophenes prepared either by electropolymerizatin or by chemical oxidative polymerization [8,15], mainly resulting from better conjugated structures of P2Se and P3Se with less structural defects as confirmed by FT-IR spectral results and also the red-shifting in the maximum absorption peak in UV-vis spectra.

In the neutral state, PSe, P2Se and P3Se all display brick-red or red in color with typical coordinates of L* = 62.72, a* = 25.42, b* = 16.91 (Inset of Fig. 5A–C & Table 2). With stepwise increase of the applied potentials, the single absorption band of polyselenophene in the visible region depletes gradually and a new absorption arises in the near-infrared region (>800 nm) because of the formation charge species upon doping. These evolution in the absorption spectra also leads to obvious color changes towards blue/baby blue (L* = 87.07, a* = −2.22, b* = 0.01) (Fig. 5A–C & Table 2). This electrochromism phenomenon of polyselenophene are also observed by previous reports [8], but unfortunately the electrochromic kinetics of parent polyselenophene has not been carefully investigated due to the poor performance of the obtained polyselenophene films.

### 3.7. Kinetic studies

To further evaluate the electrochromic performances of as-formed polyselenophene films, the kinetic studies of PSe, P2Se, and P3Se have been carried out by using a double-step chronoamperometry method. The transmittance-time profiles of these polyselenophene films are illustrated in Fig. 5D–G, and the corresponding electrochromic parameters including optical contrast, coloration efficiency and response time, are summarized in Table 3.

Due to the poor film quality, the electrochromic performance and stability of PSe is not good with the optical contrast of 28% at 1100 nm (Fig. 5D). With the improvement in the film quality, the optical contrast of P2Se and P3Se are generally improved by 2–3

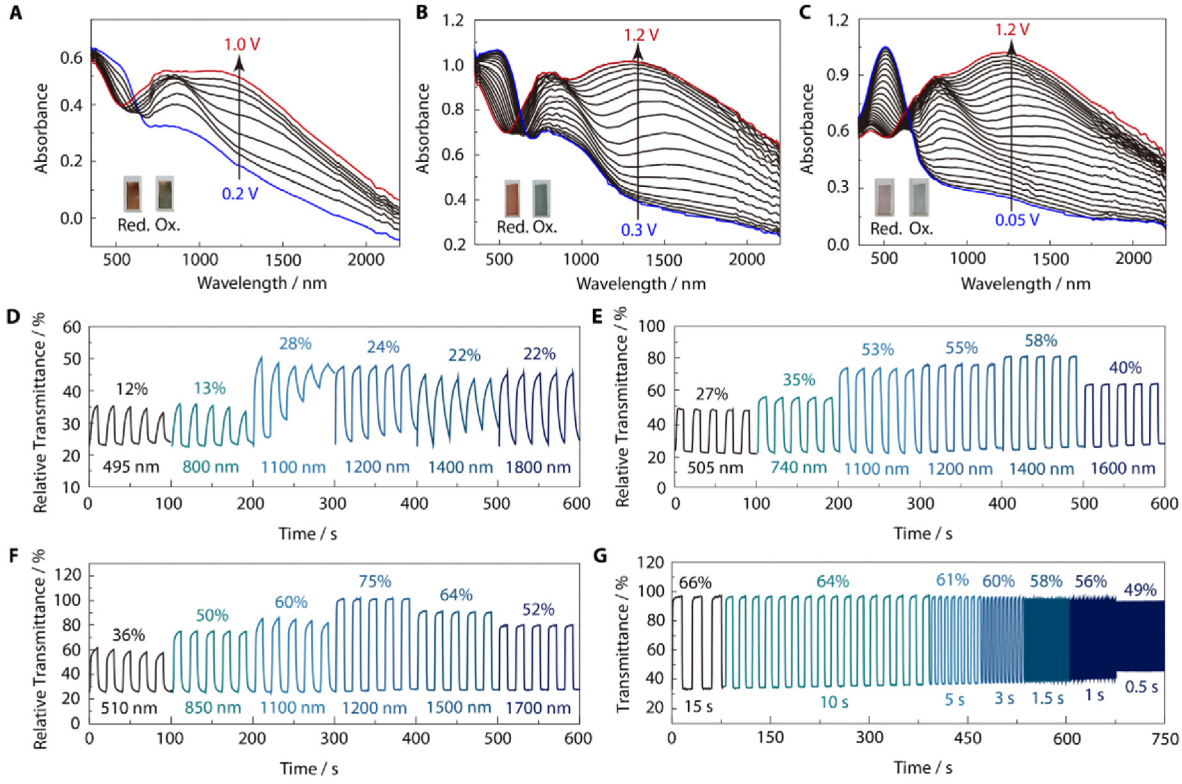


**Fig. 5. Electrochromic performances of polyselenophenes.** (A-C) Spectroelectrochemistry for PSe (A), P2Se (B) and P3Se (C) films on the ITO coated glass in blank $CH_2Cl_2$-$Bu_4NPF_6$ (0.10 mol $L^{-1}$) solution. Applied potential ranges: 0.2–1.0 V for PSe, $\Delta E$ = 0.1 V; 0.3–1.2 V for P2Se, $\Delta E$ = 0.05 V; 0.05–1.2 V for P3Se, $\Delta E$ = 0.05 V. (D-F) Time-transmittance profiles of PSe (D), P2Se (E) and P3Se (F) films recorded by double step chronoamperometry under the switching time of 10 s at different wavelengths. Applied potentials: PSe, −1.0 and 1.0 V; P2Se, −1.0 and 1.2 V; P3Se, −1 and 1.4 V. (G) Optical contrasts of P3Se (1800 nm, −1.0 and 1.0 V) recorded by double step under varying switching time intervals as indicated.

**Table 2**
Spectroelectrochemical parameters and color coordinates of PSe, P2Se, and P3Se.

| Polymer | $\lambda_{max}$ (nm) | $\lambda_{onset}$ (nm) | $E_{g,opt}$ (ev) | CIE color coordinates | | | | | |
|---|---|---|---|---|---|---|---|---|---|
| | | | | Neutral state | | | Oxidized state | | |
| | | | | L | a | b | L | a | b |
| PSe | 450 | 646 | 1.92 | 65.15 | 12.12 | 22.73 | 67.64 | −1.10 | 15.06 |
| P2Se | 505 | 667 | 1.86 | 62.72 | 25.42 | 16.91 | 69.37 | −8.96 | 1.14 |
| P3Se | 515 | 721 | 1.72 | 78.75 | 7.88 | −1.73 | 87.07 | −2.22 | 0.01 |

**Table 3**
Electrochromic parameters of different polyselenophene films at varying wavelengths.

| Polymer | Wavelength (nm) | $T_{red}$ | $T_{ox}$ | $\Delta T$ | Response time (s) | | Coloration efficiency ($cm^2/C$) |
|---|---|---|---|---|---|---|---|
| | | | | | oOx | Red | |
| PSe | 495 | 18% | 30% | 12% | 7.2 | 1.7 | 41 |
| | 800 | 33% | 20% | 13% | 2.9 | 8.4 | 15 |
| | 1100 | 70% | 42% | 28% | 5.6 | 7.4 | 40 |
| | 1200 | 55% | 31% | 24% | 3.8 | 5.6 | 57 |
| | 1400 | 74% | 52% | 22% | 8.8 | 8.7 | 89 |
| | 1800 | 64% | 42% | 22% | 6.4 | 7.3 | 115 |
| P2Se | 505 | 25% | 52% | 27% | 2.7 | 0.5 | 96 |
| | 740 | 70% | 35% | 35% | 3.8 | 2.9 | 90 |
| | 1100 | 75% | 22% | 53% | 4.6 | 2.6 | 122 |
| | 1200 | 92% | 37% | 55% | 1.4 | 1.3 | 230 |
| | 1400 | 97% | 39% | 58% | 1.2 | 1.0 | 241 |
| | 1600 | 76% | 36% | 40% | 0.8 | 0.7 | 227 |
| P3Se | 510 | 29% | 65% | 36% | 6.6 | 3.9 | 122 |
| | 850 | 53% | 3% | 50% | 3.5 | 4.6 | 169 |
| | 1100 | 88% | 28% | 60% | 2.7 | 5.2 | 224 |
| | 1200 | 95% | 20% | 75% | 1.0 | 0.9 | 450 |
| | 1500 | 96% | 32% | 64% | 0.7 | 0.5 | 370 |
| | 1700 | 89% | 37% | 52% | 0.7 | 0.4 | 245 |

times with significantly enhanced switching stability (Fig. 5E and F & Table 3). Notably, P3Se film displays superior optical contrast over 50% in the whole near-infrared region (800−1800 nm) with the highest value up to 75% at 1200 nm, comparable to excellent organic electrochromic polymers reported so far [15]. Furthermore, P2Se and P3Se also exhibit faster switching times to achieve 95% optical contrast between the oxidation and reduction processes with higher coloration efficiency (Table 3). Again, P3Se film reveals an impressive switching time of 0.7 s for oxidation and 0.4 s for reduction with the highest coloration efficiency of 450 $cm^2$ $C^{-1}$ at 1200 nm, better than most of conjugated polymers in the polythiophene family like polythiophene and PEDOT[26]. By monitoring the percent transmittance change as a function of interval time (from 15 s down to 0.5 s), P2Se and P3Se can preserve high optical contrast over 44% while maintaining good stability even at a very short switching time of 0.5 s, much better than PSe (Figs. 5G & S10). Moreover, no obvious transmittance changes in the neutral state can be observed from the open-circuit memory of P2Se and P3Se films monitored at 1100 nm, while mild fluctuations of less than 5% variation occur in their oxidized state (Fig. S11).

Overall, the electrochromic performance of polyselenophene can be significantly enhanced by extending the monomeric precursor from Se to 3Se to yield high-quality polyselenophene film with better conjugated structure and less defects via low-potential electropolymerization. Additionally, P3Se film exhibit excellent electrochromic performance with superior optical contrast, fast switching time, high coloration efficiency, as well as good stability, which are comparable to advanced electrochromic materials including inorganic compounds, small organic molecules, and other high-performance conjugated polymers [3,4], making it a good material candidate for various electrochromic devices.

### 3.8. Flexible electrochromic devices

Flexible electrochromic devices have been extensively employed in many applications, such as color-changing tattoos and e-papers[45,46]. Enabled by the high performance of P2Se and P3Se and the ease of patterning via electropolymerization, we can successfully fabricate flexible electrochromic devices with the configuration of ITO-PET/patterned polyselenophene layer/gel electrolyte/ITO-PET. As shown in Fig. 6, patterned flexible electrochromic devices of our university “JXSTNU” with P2Se or P3Se as the functional layer display reversible color-changing phenomenon upon doping/dedoping at low driving potentials of −1.0 and 1.0 V. These devices are foldable, and show good stability against both redox cycling and mechanical bending/relaxing, which are appealing for wearable electronic technologies, and thus can serve to revolutionize electrochromic applications towards deformable electronics.

## 4. Conclusion

In this work, the effect of precursor chain length on the electropolymerization behavior and the optoelectronic performances of the resultant polyselenophene films has been systematically investigated by using various characterization methods including electrochemical, spectral, morphological, together with quantum calculations. Stepwise increase in chain length of the precursors from Se to 3Se leads to much lowered onset oxidation potentials, affording low-potential electropolymerization to achieve high quality polyselenophene films with better conjugated structures and less structural defects. The resultant P2Se and P3Se films exhibit much enhanced optoelectronic properties such as better redox activity and stability, lowered optical band gaps, higher

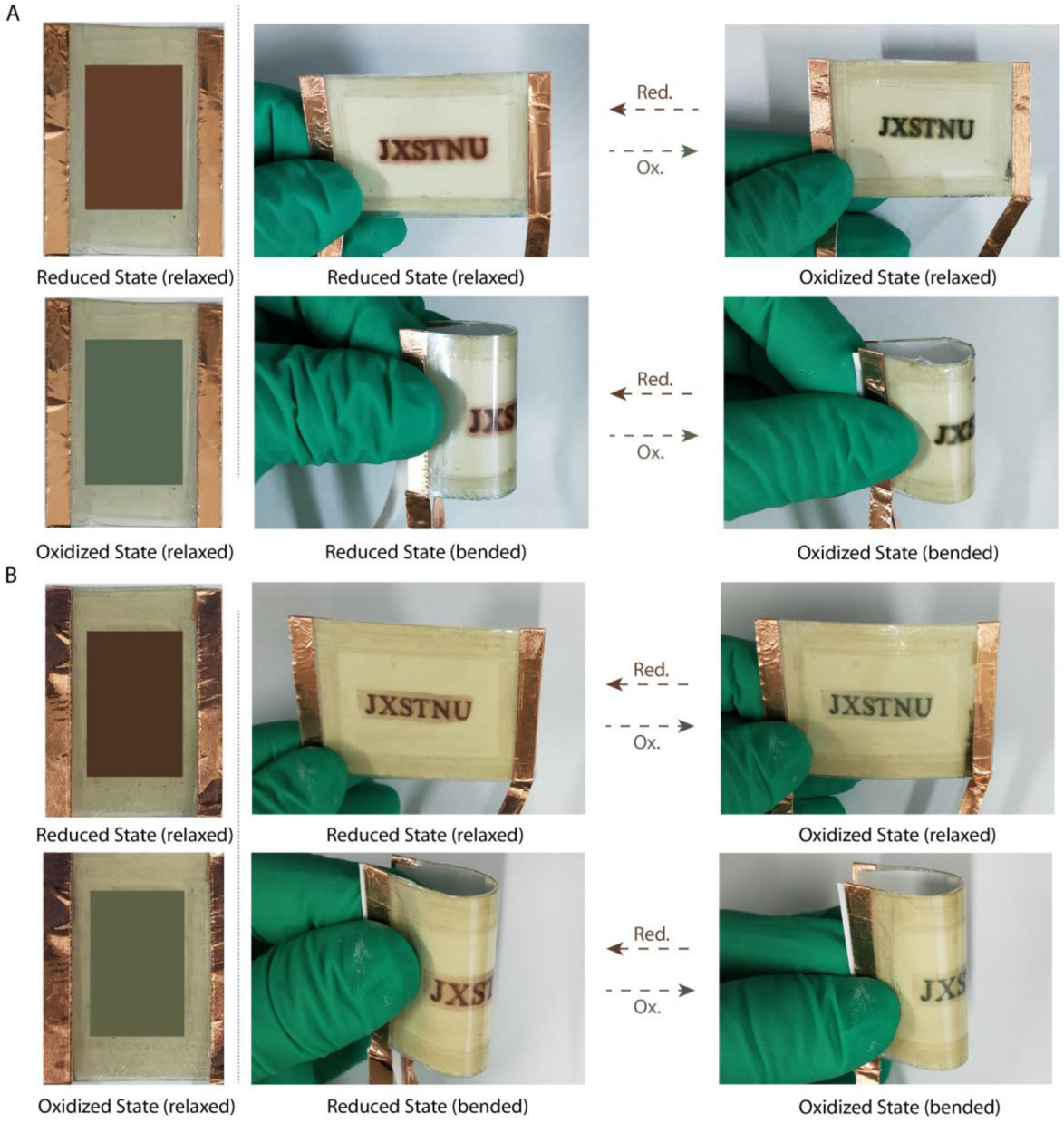


**Fig. 6. Polyselenophene-based flexible electrochromic devices.** (A, B) Color changing digital images for P2Se (A) or P3Se (B)-based flexible electrochromic devices under relaxing and bending conditions. (For interpretation of the references to color in this figure legend, the reader is referred to the Web version of this article.)

electrochromic performances. Enabled by these advantageous properties, patterned flexible electrochromic devices have been fabricated with electrodeposited polyselenophene films, and these devices reveal reversible and stable color changes upon both doping-dedoping and mechanical bending.

## Declaration of competing interest

The authors declare that they have no conflicts interests. All the authors listed and the responsible authorities where the work was carried out have approved the manuscript that is enclosed.

## CRediT authorship contribution statement

**Baoyang Lu:** Conceptualization, Methodology, Writing - review & editing. **Nannan Jian:** Data curation, Writing - original draft. **Ximei Liu:** Supervision. **Jingkun Xu:** Supervision. **Guoqun Zhao:** Supervision.

## Acknowledgements

This work was supported by the National Natural Science Foundation of China (Grant No. 51763010 & 51963011), Technological Expertise and Academic Leaders Training Program of Jiangxi Province (Grant No. 20194BCJ22013), Double Thousand Talents Plan in Jiangxi Province - Youth Program, the Science and Technology Research Program of Jiangxi Educational Committee (Grant No. GJJ190622), and Research Project of the State Key Laboratory of Mechanical System and Vibration (Grant No. MSV202013).

## Appendix A. Supplementary data

Supplementary data to this article can be found online at https://doi.org/10.1016/j.electacta.2020.135974.

## References


[1] D. Khim, A. Luzio, G.E. Bonacchini, G. Pace, M.J. Lee, Y.Y. Noh, M. Caironi, Uniaxial alignment of conjugated polymer films for high-performance organic field-effect transistors, Adv. Mater. 30 (2018), 1705463.

[2] B.W. Xu, J.H. Hou, Solution-processable conjugated polymers as anode interfacial layer materials for organic solar cells, Adv. Energy Mater. 8 (2018), 1800022.

[3] P.M. Beaujuge, J.R. Reynolds, Color control in pi-conjugated organic polymers for use in electrochromic devices, Chem. Rev. 110 (2010) 268–320.

[4] K.W. Lin, S. Chen, B.Y. Lu, J.K. Xu, Hybrid π-conjugated polymers from dibenzo pentacyclic centers: precursor design, electrosynthesis and electrochromics, Sci. China B: Chemistry 60 (2017) 38–53.

[5] H. Yuk, B.Y. Lu, X.H. Zhao, Hydrogel bioelectronics, Chem. Soc. Rev. 48 (2019) 1642–1667.

[6] B.Y. Lu, H. Yuk, S.T. Lin, N.N. Jian, K. Qu, J.K. Xu, X.H. Zhao, Pure PEDOT:PSS hydrogels, Nat. Commun. 10 (2019) 1043.

[7] F.Q. Hu, Y. Xue, J.K. Xu, B.Y. Lu, PEDOT-based conducting polymer actuators, Front. Robot. AI 6 (2019) 114.

[8] A. Patra, M. Bendikov, Polyselenophenes, J. Mater. Chem. 20 (2010) 422–433.

[9] A. Patra, M. Bendikov, S. Chand, Poly(3,4-ethylenedioxyselenophene) and its derivatives: novel organic electronic materials, Acc. Chem. Res. 47 (2014) 1465–1474.

[10] M.F.G. Klein, F.M. Pasker, S. Kowarik, D. Landerer, M. Pfaff, M. Isen, D. Gerthsen, U. Lemmer, S. Hoeger, A. Colsmann, Carbazole-phenyl-benzotriazole copolymers as absorber material in organic solar cells, Macromolecules 46 (2013) 3870–3878.

[11] K. Li, Z. Li, K. Feng, X. Xu, L. Wang, Q. Peng, Development of large band-gap conjugated copolymers for efficient regular single and tandem organic solar cells, J. Am. Chem. Soc. 135 (2013) 13549–13557.

[12] B.Y. Lu, S. Chen, J.K. Xu, G.Q. Zhao, Thermoelectric performances of different types of polyselenophene and its copolymers with 3-methylthiophene via electropolymerization, Synth. Met. 183 (2013) 8–15.

[13] B.Y. Lu, S.L. Ming, K.W. Lin, S.J. Zhen, H.T. Liu, H. Gu, S. Chen, Y.Z. Li, Z.Y. Zhu, J.K. Xu, [1,2,5]Chalcogenodiazolo[3,4-c]pyridine and selenophene based donor–acceptor–donor electrochromic polymers electrosynthesized from high fluorescent precursors, New J. Chem. 40 (2016) 8316–8323, https://doi.org/10.1039/C5NJ03432A.

[14] S.Z. Pu, J. Hou, J.K. Xu, G.M. Nie, S.S. Zhang, L. Shen, Q. Xiao, Electrosyntheses of freestanding and conducting polyselenophene films, Mater. Lett. 59 (2005) 1061–1065.

[15] J.K. Xu, J. Hou, S.S. Zhang, G.M. Nie, S.Z. Pu, L. Shen, Q. Xiao, Electrosyntheses of high quality freestanding polyselenophene films in boron trifluoride diethyl etherate, J. Electroanal. Chem. 578 (2005) 345–355.

[16] B. Dong, Y.H. Xing, J.K. Xu, L.Q. Zheng, J. Hou, F. Zhao, Electrosyntheses of free-standing and highly conducting polyselenophene films in an ionic liquid, Electrochim. Acta 53 (2008) 5745–5751.

[17] Y. Sun, S.C. Chien, H.L. Yip, Y. Zhang, K.S. Chen, D.F. Zeigler, F.C. Chen, B. Lin, A.K.Y. Jen, High-mobility low-bandgap conjugated copolymers based on indacenodithiophene and thiadiazolo 3,4-c pyridine units for thin film transistor and photovoltaic applications, J. Mater. Chem. 21 (2011) 13247–13255.

[18] S.G. Xu, Y.L. Liu, J.H. Li, Y.B. Wang, S.K. Cao, Synthesis and characterization of low-band-gap conjugated polymers containing phenothiazine and benzo-2,1,3-thia-/seleno-diazole, Polym. Adv. Technol. 21 (2010) 663–668.

[19] S.L. Ming, S.J. Zhen, K.W. Lin, L. Zhao, J.K. Xu, B.Y. Lu, Thiadiazolo 3,4-c pyridine as an acceptor toward fast-switching green donor-acceptor-type electrochromic polymer with low bandgap, ACS Appl. Mater. Interfaces 7 (2015) 11089–11098.

[20] S.L. Ming, S.J. Zhen, X.M. Liu, K.W. Lin, H.T. Liu, Y. Zhao, B.Y. Lu, J.K. Xu, Chalcogenodiazolo 3,4-c pyridine based donor-acceptor-donor polymers for green and near-infrared electrochromics, Polym. Chem. 6 (2015) 8248–8258.

[21] H. Gu, S.L. Ming, K.W. Lin, S. Chen, X.M. Liu, B.Y. Lu, J.K. Xu, Isoindigo as an electron-deficient unit for high-performance polymeric electrochromics, Electrochim. Acta 260 (2018) 772–782.

[22] N.N. Jian, H. Gu, S.M. Zhang, H.T. Liu, K. Qu, S. Chen, X.M. Liu, Y.F. He, G.F. Niu, S.Y. Tai, J. Wang, B.Y. Lu, J.K. Xu, Y. Yu, Synthesis and electrochromic performances of donor-acceptor-type polymers from chalcogenodiazolo 3,4-c pyridine and alkyl ProDOTs, Electrochim. Acta 266 (2018) 263–275.

[23] G.S. Collier, I. Pelse, J.R. Reynolds, Aqueous electrolyte compatible electrochromic polymers processed from an environmentally sustainable solvent, ACS Macro Lett. 7 (2018) 1208–1214.

[24] D. Yigit, S.O. Hacioglu, M. Gullu, L. Toppare, Synthesis and spectroelectrochemical characterization of multi-colored novel poly(3,6-dithienylcarbazole) derivatives containing azobenzene and coumarin chromophore units, Electrochim. Acta 196 (2016) 140–152.

[25] Y.P. Wen, J.K. Xu, Scientific importance of water-processable PEDOT-PSS and preparation, challenge and new application in sensors of its film electrode: A review, J. Polym. Sci., Part A: Polym. Chem. 55 (2017) 1121–1150, https://doi.org/10.1002/pola.27973.

[26] S.J. Zhen, J.K. Xu, B.Y. Lu, S.M. Zhang, L. Zhao, J. Li, Tuning the optoelectronic properties of polyfuran by design of furan-EDOT monomers and free-standing films with enhanced redox stability and electrochromic performances, Electrochim. Acta 146 (2014) 666–678.

[27] Z.X. Xue, N. Gao, Y. Xue, B.Y. Lu, O. Waston, L. Zang, J.K. Xu, Structural design and applications of stereoregular fused thiophenes and their oligomers and polymers, Polym. Rev. (2019), https://doi.org/10.1080/15583724.2019.1673404.

[28] W.S. Li, Y.T. Guo, J.J. Shi, H.T. Yu, H. Meng, Solution-processable neutral green electrochromic polymer containing thieno 3,2-b thiophene derivative as unconventional donor units, Macromolecules 49 (2016) 7211–7219.

[29] W. Chen, G. Xue, Low potential electrochemical syntheses of heteroaromatic conducting polymers in a novel solvent system based on trifluroborate-ethyl ether, Prog. Polym. Sci. 30 (2005) 783–811.

[30] N.N. Jian, K. Qu, H. Gu, L. Zou, X.M. Liu, F.Q. Hu, J.K. Xu, Y. Yu, B.Y. Lu, Highly fluorescent triazolopyridine-thiophene D-A-D oligomers for efficient pH sensing both in solution and in the solid state, Phys. Chem. Chem. Phys. 21 (2019) 7174–7182.

[31] N.N. Jian, K.W. Lin, B. Guo, G. Zhang, X.M. Liu, L. Zou, B.Y. Lu, J.K. Xu, A reusable fluorescent sensor from electrosynthesized water-soluble oligo(1-pyrenesulfonic acid) for effective detection of $Fe^{3+}$, New J. Chem. 1 (2018) 19450–19457.

[32] D. Bhattacharyya, K.K. Gleason, Low band gap conformal polyselenophene thin films by oxidative chemical vapor deposition, J. Mater. Chem. 22 (2012) 405–410.

[33] A. Ghosh, R. Gonnade, M. Ravikanth, Rhenium(I) tricarbonyl complex of 5,20-bis(p-tolyl)-10,15-bis(p-methoxyphenyl)-21-selenaporphyrin: first X-ray structural characterization of metal complex of 21-selenaporphyrin, Dalton Trans. 42 (2013) 10798–10806.

[34] C.X. Chen, Z.Y. Gan, K. Zhou, Z. Ma, Y.Q. Liu, Y.H. Gao, Catalytic polymerization of N-methylthionine at electrochemically reduced graphene oxide electrodes, Electrochim. Acta 283 (2018) 1649–1659.

[35] S.X. Xiong, J.P. Lan, S.Y. Yin, Y.Y. Wang, Z.Z. Kong, M. Gong, B.H. Wu, J. Chu, X.Q. Wang, R.L. Zhang, Y.G. Li, Enhancing the electrochromic properties of polyaniline via coordinate bond tethering the polyaniline with gold colloids, Sol. Energy Mater. Sol. Cell. 177 (2018) 134–141.

[36] Y.E. Firat, A. Peksoz, Efficiency enhancement of electrochromic performance in NiO thin film via Cu doping for energy-saving potential, Electrochim. Acta 295 (2019) 645–654.

[37] Z.J. Fu, Z.Y. Ma, T. Yu, L.H. Bi, A first blue fluorescence composite film based on graphitic carbon nitride nanosheets/polyoxometalate for application in reversible electroluminescence switching, J. Mater. Chem. C 7 (2019) 3253–3262.

[38] B.C. Ozkan, T. Soganci, H. Turhan, M. Ak, Investigation of rGO and chitosan effects on optical and electrical properties of the conductive polymers for advanced applications, Electrochim. Acta 295 (2019) 1044–1051.

[39] M. Abdulrazzaq, M.I. Ozkut, G. Gokce, S. Ertan, E. Tutuncu, A. Cihaner, A low band gap polymer based on selenophene and benzobis (thiadiazole), Electrochim. Acta 249 (2017) 189–197.

[40] H.Y. Chen, S.C. Yeh, C.T. Chen, C.T. Chen, Comparison of thiophene- and selenophene-bridged donor-acceptor low band-gap copolymers used in bulk-heterojunction organic photovoltaics, J. Mater. Chem. 22 (2012) 21549–21559.

[41] B. Ballarin, M. Lanzi, L. Paganin, G. Cesari, Electrochemical synthesis and characterization of poly 3-(omega-bromoalkyl)thiophenes, Electrochim. Acta 52 (2007) 4087–4091.

[42] T. Ikeda, Y. Nagata, Y. Zheng, D. Liu, H.J. Butt, M. Shimoda, Electrochemically durable thiophene alkanethiol self-assembled monolayers, Langmuir 30 (2014) 1536–1543.

[43] C. Moorlag, O. Clot, M.O. Wolf, B.O. Patrick, Switchable thiophene coordination in Ru(II) bipyridyl phosphinoterthiophene complexes, Chem. Commun. 24 (2002) 3028–3029.

[45] M. Gratzel, Ultrafast colour displays, Nature 409 (2001) 575–576.

[46] X.X. Liu, A. Zhou, Y.B. Dou, T. Pan, M.F. Shao, J.B. Han, M. Wei, Ultrafast switching of an electrochromic device based on layered double hydroxide/prussian blue multilayered films, Nanoscale 7 (2015) 17088–17095.

[47] B.Y. Lu, Y.Z. Li, J.K. Xu, Electropolymerization study of benzothiophenes and characterization of novel poly(dibenzothiophene-S,S-dioxide), J. Electroanal. Chem. 643 (2010) 67–76, https://doi.org/10.1016/j.jelechem.2010.03.007.